PCCP

Accepted Manuscript

ROYAL SOCIETY OF CHEMISTRY

www.rsc.org/pccp

Influence of surface functionalization on the hydrophilic character of mesoporous silica nanoparticles

G. E. Musso [a], E. Bottinelli[a], L. Celi [b], G. Magnacca[a] and G. Berlier[a1]

[a]Università di Torino, Dipartimento di Chimica and NIS Centre, Via P. Giuria 7, 10125 Torino, Italy

[b]Università di Torino, Dipartimento di Scienze Agrarie, Forestali e Alimentari, Via Leonardo da Vinci, 44 - 10095 Grugliasco (TO), Italy

---

[1]Corresponding author: e-mail: gloria.berlier@unito.it; Tel. 0039 0116707856; Fax: 0039 0116707953

Abstract

We report about the synthesis and surface functionalization of MCM-41 like mesoporous silica nanoparticles (MSNs) with spheroidal shape and particle size of 141 ± 41 nm. The success of surface functionalization with aminopropyl and sodium ethylcarboxylate groups (giving amino-MSN and carboxy-MSN, respectively) was ascertained by infrared spectroscopy and ζ potential measurements. The former showed the decrease of surface silanol groups and the corresponding appearance of signals related to NH_2 bending mode (δNH_2) at 1595 cm^{-1} and COO^- stretching (ν_{as} and ν_{sym}) at 1562 and 1418 cm^{-1}. The latter showed a change in surface charge, in that the isoelectric point, IEP, changed from pH 3-4.5 to 8.5 when MSN was functionalized with the amino groups, while carboxy-MSN showed a more negative charge in the whole pH range with respect to MSN. The hydrophilic character of the prepared materials was ascertained by quantitative microgravimetric measurements, allowing the calculation of the average isosteric adsorption heat ($\bar{q}_{st}$). This was found to be 51 ± 3 kJ/mol for MSN, 61 ± 4 and 65 ± 3 kJ/mol for amino- and carboxy-MSN samples, respectively. The increase in $\bar{q}_{st}$ after functionalization can be ascribed to the specific interaction of water molecules with the functionalizing agents, in agreement with a higher basicity with respect to silanol groups. Moreover, the possibility of multiple H-bonding interactions of water molecules with the carboxylate anion is put forward to account for the higher water uptake with respect to parent MSN.

Introduction

Since from the pioneering work of Prof. Vallet-Regí in 2001,[1] the number of publications related to the use of mesoporous silica materials as drug delivery systems (DDS) or related applications in the biomedical field has increased exponentially.[2-8] The reasons for this success are easily understood on the basis of the well-known properties of the material, including extremely high specific surface area (around 1000 m^2/g), ordered porosity with narrow pore size distribution and large pore volume, together with the possibility to modulate pore size, allowing the accommodation of molecules with different sterical hindrance, which are ideal properties for high drug loading and diffusion-driven gradual release.[2, 9, 10]

Another important aspect explaining the impressive interest in the field of mesoporous silica is related to the possibility to obtain the materials in form of nano- and submicrometer-sized particles, commonly referred to as mesoporous silica nanoparticles (MSNs).[3, 11-13] In this form MSNs can be passively transported in physiological fluids, for instance in the case of extravasation from leaky tumour vessels, making therapeutic delivery into disease cells more efficient whereas the exposure of healthy tissue to toxic side effects lowers.[14] Accordingly, many studies are being carried out to follow the mechanisms of interaction and internalization in cells.[11, 15-17]

Moreover, the Si-OH rich silica surface can be easily functionalized with suitable reactants. This could be aimed at i) optimizing the interaction with drugs,[18, 19] ii) covalently linking agents for targeted delivery,[20, 21] iii) modifying surface charge and properties affecting the interaction with biomolecules (protein, bacteria, etc) or iv) improving permeability through cellular membranes.[22, 23] All these aspects have led to the concept of MSNs as pharmaceutically adapted platforms.[24] The platform concept is based on the possibility to obtain multifunctional nanocarriers for delivering therapeutic and diagnostic (theranostics) agents (*e.g.* drugs, siRNA, imaging probes, etc).[21, 25]

Notwithstanding all the above mentioned aspects, and the intense research activity, many aspects regarding the use of MSNs in the fields of nanobiotechnology and nanomedicine are still unsolved. Silica is expected to have relatively good stability and biocompatibility, even if its fate in physiological fluids[4, 26]and the actual effect on cells are still the object of many studies.[27] The fate of nanomaterials in biological and environmental conditions is related to many aspects,[28] including hydrophobicity/hydrophilicity,[23] size and shape,[16, 17, 29] surface charge and surface functionalization.[23, 30, 31]

Intravenous injection is the most common entrance of most nanoparticles applied in biomedicine. This means that MSNs, as other nanoparticles, will reach the bloodstream and interact with blood components. With this respect, in vivo toxicity of MSNs can be tested by evaluating their interaction with blood components, such as red blood cells (RBC) and serum proteins.[32, 33] More specifically, non-specific protein adsorption needs to be considered, since it can promote phagocytosis by making the MSN visible to phagocytic cells. This could result in their rapid clearance from the blood stream before they reach their target, with consequent decrease in efficiency. On the other hand, the formation of protein corona on MSNs has been reported to extremely depress their haemolytic activity in RBCs,[32] and this was found to be strictly related to the nature of surface functionalization.[33] The unraveling of the ensemble of surface processes and phenomena actually occurring *in vivo* is still a challenge, but there is a general consensus about the important role of i) biomaterial surface structure, ii) states of adsorbed water molecules, and iii) states of adsorbed proteins.[34, 35] These constitute a major element of the biological identity on the surface of nanoparticles. In this respect, the study of water interaction with the surface of biomaterials has been reported, as a first step of a research aimed to investigate factors affecting the interaction with proteins.[35, 36]

Aim of this work is the production and characterization of MCM-41-like MSN functionalized with amino (-$C_3H_6NH_2$) and sodium carboxylate (-C_2H_4COONa) groups (amino- and carboxy-MSN, respectively), covalently bonded by post-synthesis grafting. The two different functional groups were selected in order to investigate the effect of functionalization on the surface properties of the materials, particularly regarding its surface charge and hydrophilic character. This knowledge is in fact important to modulate these properties as a function of the environment (*i.e.* impregnating solutions for drug loading and release, physiological fluids, formation of protein corona which modulates their biological identity etc). This would also imply a better understanding of the fate of this important biomaterial in physiological fluids, both *in vitro* and *in vivo*. At the best of our knowledge, this information is still missing, although the literature on silica-based materials (both porous and not porous, amorphous and crystalline) is abundant.[37-54]

This aim was pursued by performing quantitative water adsorption measurements by microgravimetry, complemented by a general physico-chemical characterization of the samples. This included the measurement of surface charge as a function of pH, a qualitative monitoring of water interaction with the surface of dehydrated samples by *in situ* infrared spectroscopy, and the calculation of the water isosteric heat of adsorption.

2. Experimental section

2.1 Synthesis

All reactants and solvents were purchased from Sigma-Aldrich, except carboxyethylsilanetriol sodium salt, 25% in water (ABCR, Germany). All chemicals were employed as received without further purification. Sipernat 320 amorphous silica was supplied by Evonik Degussa.

MCM-41 MSN was prepared by using cetyltrimethylammonium bromide (CTAB) as structure directing agent (SDA) according to a slightly modified literature procedure.[11, 55] Carboxy-MSN and amino-MSN samples were prepared by post-synthesis grafting employing carboxyethylsilanetriol sodium salt and 3-aminopropyl triethoxysilane (APTS), respectively, by modifying literature procedures.[56,57,58] Details can be found in Supporting Information.

2.2. Characterization

Powder X Ray Diffraction (PXRD) patterns were collected with a PW3050/60 X'Pert PRO MPD diffractometer (Panalytical) working in Bragg–Brentano geometry, using Cu Kα radiation (40 mA and 45 kV), with a scan speed of 0.01° min^{-1}. High Resolution Transmission Electron Microscopy (HRTEM) analyses were performed by means of a JEM 3010-UHR microscope (JEOL Ltd.) operating at 300 kV. For the measurements, MSNs powders were dispersed on a copper grid coated with a perforated carbon film. The size distributions of the samples were obtained by measuring a statistically representative number of particles (ca. 200 particles) and the results are indicated as mean particle diameter (dm) ± standard deviation (STD) (dm±STD).

Specific surface area (SSA), cumulative pore volume and pore size distribution of the RT overnight outgassed samples were measured by N_2 adsorption-desorption isotherms at liquid nitrogen temperature (LNT) using an ASAP 2020 physisorption analyzer (Micromeritics). The SSA was calculated by the Brunauer-Emmett-Teller (BET) method and the average pore size was determined by means of the Barrett-Joyner-Helenda (BJH) method, employing Kruk–Jaroniec–Sayari (KJS) equation (the most reliable model for porosity assessment on MCM-41 like materials) on the adsorption branch of nitrogen isotherms. Pore wall thickness was calculated by the measure of the d_{100} distance estimated by XRD, with the formula:

$$a = d/\cos(\theta)$$

where *a* is the fundamental lattice vector, the length of which corresponds to the center-to-center distance of the pores. Wall thickness *e* is calculated as the difference between *a* and the pore diameter estimated by BJH analysis.[59, 60]

Thermogravimetric analysis (TGA) was carried out on a Q600 analyzer (TA Instruments) heating the samples at a rate of 10 °C/min from 30 °C to 1000 °C in a nitrogen flow. Before starting measurements, samples were equilibrated at 30 °C. Once reached the final temperature an isotherm was run for 15 min in air to burn the hydrocarbon residues. The C, H, N content was determined using a Thermo Electron Corporation CHNS-O analyzer. The surface density of functional groups calculated by this technique was corrected to the sample dry weight by considering the amount of adsorbed moisture/impurities measured by TGA.

The electrophoretic mobility of the synthesized samples was measured as a function of pH in an aqueous solution. The ionic strength was kept constant by dispersing 10.0 mg of each powdered sample in 10 ml of KCl 0.01 M solution, employed as supporting electrolyte. Appropriate volumes of HCl or KOH solutions were added in order to obtain for each MSN sample a suspension series with different pH values ranging from 2 to 10. To maintain the final volume of all suspensions constant, HCl and KOH solutions with different concentrations (from 1M to 0,01M) were used. All samples were prepared in duplicated. The samples were vigorously stirred for few minutes and left for about 16 hours at room temperature to reach equilibration. Then all suspensions were sonicated for a few minutes before measurements. The resulting electric conductivity was 1.29 ± 0.14 mS cm^{-1}. pH was measured electrometrically. The electrophoretic mobility was measured by Laser Doppler Velocimetry - Photon Correlation Spectroscopy using a DELSA 440 spectrometer (Beckman Coulter, Inc.) equipped with a 5 m W HeNe laser (632.8 nm). The electrophoretic mobility data were converted to zeta potential (ζ) using the Smoluchowski equation.[61]

Fourier Transform infrared (FTIR) spectra were recorded using a Vertex70 spectrometer (Bruker Optics) equipped with a DTGS detector, working with a resolution of 4 cm^{-1} over 64 scans. The spectra were obtained in transmission mode, with the samples pressed in the form of self-supporting pellets mechanically protected with a pure gold frame. Samples were placed in quartz cells equipped with KBr windows, allowing *in situ* activation, measurements and water vapour dosage. Before the measurements the samples were outgassed at RT for 2 hours to remove adsorbed water and impurities. Water vapour pressure was measured after equilibration with the sample with Pirani thermal conductivity gauges. All the prepared pellets showed similar thickness (*ca* 5.5

mg/cm^2), so that the intensity of the reported spectra can be directly compared on a semi-quantitative ground without further normalization.

Microgravimetric H_2O adsorption/desorption isotherms were measured with an intelligent gravimetric analyzer (IGA-002, Hiden Analytical), based on an ultrahigh-vacuum (UHV) microbalance (weighing resolution of 0.2 μg) with integrated temperature and pressure control. Temperature control was based on a thermostated water bath/circulator, while pressure control was achieved with a Baratron capacitance manometer (accuracy ± 0.05 mbar). Buoyancy corrections were carried out using the weights and densities of all the components of the sample (including adsorbed phase) and counterweight sides of the balance and the measured temperature. The mass uptake was measured as a function of time, and the approach to equilibrium of the mass relaxation curve was monitored in real time using a computer algorithm (real time processor RTP). For each isotherm point the time origin of real-time analysis was set at 95% of the pressure change, while the minimum and maximum data collection time were set to 10 and 120 mins respectively. RTP uses last-squares regression of a linear driving force (LDF) model in order to extrapolate a value of the mass relaxation asymptote and assess the time-scale of interaction. The samples were loaded in a sealed stainless steel reactor, where they were outgassed at 50°C for 6 hours prior to H_2O dosage, in order to measure the sample dry weight. The adsorption isotherms were measured varying the water equilibrium pressure in the 0-10 mbar interval (step 1.5 mbar) at 25, 35 and 50 °C. For each temperature 4 scans (2 adsorption and 2 desorption) were carried out.

The isosteric heat of adsorption q_{st} was calculated by employing the Clausis-Clapeyron equation:

$$(\ln p)_\theta = \frac{q_{st}}{R}\left(\frac{1}{T}\right)_\theta + \cos t \qquad (1)$$

by determining the slope of the best-fit line for *lnp* (*p* being H_2O equilibrium pressure at a given temperature, expressed in bar) versus*1/T* (average temperature measured on the sample during the isotherm, in K), at fixed coverage θ (*i.e.* adsorbed water amount).

3. Results and discussion

3.1 General properties of the samples

A sample of mesoporous silica nanoparticles (MSN) and two post-synthesis functionalized ones, carboxy-MSN and amino-MSN (see Experimental section and Supporting Information for details about synthesis and functionalization procedures) were characterized for their general properties, including textural and morphological features. The samples are composed by spheroidal nanoparticles (particle size 141 ±44 nm) with a regular array of channels, as seen in HRTEM images (Figure 1). The mesostructure shows the hexagonal symmetry typical of the MCM-41 system, as also testified by XRD results, displaying the typical (100), (110), (200) and (210) peaks related to the P6mm symmetry group (Figure S1). Post-synthesis functionalization caused a modification of the intensity and position of the diffraction peaks, suggesting an inclusion of the grafted moieties within the pores. More in detail, a decrease of d_{100} parameter was observed in the order MSN>amino-MSN>carboxy-MSN (Figure S1 and Table 1). Post-synthesis functionalization also affected textural properties of MSN, in that both amino- and carboxy-MSN show smaller SSA, pore volume and pore size with respect to the pristine material (Table 1), while retaining the regular mesoporous structures (type IV isotherms in FigureS2). The wall thickness parameter, calculated by combining the d_{100} values with the average pore diameter measured by gas-volumetric measurements (BJH pore diameter), increased after functionalization (6thcolumn of Table 1). These data are in good agreement with recent measurements of pore wall thickness and with HRTEM images (Figure 1).[60] All these data suggest a relatively homogeneous distribution of the grafting agents, even if it is well known that post-synthesis grafting is likely to result in a higher concentration of functional groups at the pores entrance.

Important information about the prepared materials is the density of the surface groups, which could be available for interaction with water, drugs, bioactive molecules or proteins. These are silanols (Si-OH) in the case of MSN material, plus aminopropyl (-$C_3H_6NH_2$) or sodium ethylcarboxylate (-C_2H_4COONa) groups in the case of amino- or carboxy-MSN, respectively. The determination of OH surface density in oxides is not a trivial task, as shown by the rich debate on the subject, especially when porous materials are considered.[39, 43, 44, 62-67] In this work, this estimation was obtained on the MSN sample by employing TG analysis, as proposed in Refs. [43, 44]. The OH surface density of sample MSN was calculated by measuring its weight loss during a ramp in nitrogen from 150 °C to 1000 °C (Figure 2). The gradual weight decrease in this range (5.4 wt%) can be related to surface dehydroxylation, allowing to estimate a surface density of 3.3 OH/nm^2. This value, only reported for semi-quantitative considerations, is in fairly good agreement with what reported for mesoporous silica-based samples showing a similar pattern in the infrared OH stretching region (4.5 OH/nm^2, see below).[38, 43, 68, 69] For comparison, we also mention the corresponding value calculated for a reference material, precipitated silica Sipernat 320 (Figure S3). In this case, the weight loss measured in the same range by TGA (3.9 wt%, Figure S3a) corresponds to a surface density of 15.1 OH/nm^2. Specific surface area measurements of this material are reported in Figure S3b, and the corresponding values are resumed in Table 1 for comparison.

TG analysis was also employed to estimate the amount of grafted functional groups in amino- and carboxy-MSN samples. As for MSN, the decomposition profiles were normalized to the weight of the dry samples, that is after removal of adsorbed moisture or impurities in the 30-150 °C range (Figure 2). For both samples three regions can be observed. The first one, which ranges from 150 to ~420 ºC for carboxy-MSN and from 150 to ~500 ºC for amino-MSN was ascribed by Jaroniec et al. to the loss of silanol groups on the basis of combined TG/DSC analysis.[70] These Si-

OH could be both from the silica surface (groups unaffected by the grafting procedure) and both linked to the Si atom of mono- (-Si(OH)$_2$R) or bi-legged (=Si(OH)R, R = -$C_3H_6NH_2$)alkylsiloxanegroups.[68, 71-73] The second one has a steeper slope and goes from ~420 ºC to ~600 ºC for carboxy-MSN and from ~500 ºC to ~700 ºC for amino-MSNPs. This region results from decomposition of bonded phase and can be employed to calculate the amount of grafted functional groups.[70, 74] The third gradual weight loss in the range 600/700-1000 ºC is ascribed to further dehydroxylation of Si-OH groups. Finally, the vertical loss at 1000 °C is related to the isotherm in air, causing the combustion of residual hydrocarbons adsorbed on the silica surface. The corresponding amount was included in the calculation of the grafted organic groups.

The surface density of functional groups measured by TGA was checked by CHN elemental analysis (Table 1). The measured values were corrected to the weight of the dry samples, by considering the amount of adsorbed moisture and impurities calculated from TGA (initial weight of the sample minus weight of the sample after activation at 150 °C). These values are in good agreement with TGA estimations, supporting the validity of the employed approach.

Zeta (ζ) potential measurements were performed in aqueous suspensions as a function of pH at constant ionic strength in order to determine the electrokinetic charge of the materials, and the corresponding curves are shown in Figure 3. ζ potential measurements are mainly probing the surface potential at the slipping plane located just outside the outer surface of the particles. The isoelectric point, IEP, of MSN is in the 2.5-4.5 pH range, in accordance with literature values for amorphous and mesoporous silica.[19, 22] With pH increasing ζ potential becomes more negative as a result of progressive dissociation of Si-OH groups, reaching values of -30mV, similar to those obtained for other silica-based surfaces.[19, 22, 75]

After functionalization of MSN with aminopropyl groups the surface undergoes a reversal of charge from negative to positive, ζ potential being around + 44 mV in the range of pH between 2.0 and 6.0, due to the full dominance of protonated NH_3^+groups on the surface.[19, 76, 77] This suggests the dominance of the protonated form with respect to the neutral NH_2 in a large range of pH up to 7-8, in agreement with the pKa of the aminopropyl which is 9.8. At higher pHs the ζ potential of amino-MSN samples decreased to -30 mV with a point of zero charge at pH 8.5. The rapid decline of ζ potential and the achievement of a charge similar to that of MSN confirmed the presence of residual dissociated silanols.

In the case of carboxy-MSN sample, no IEP could be observed, since the material shows negative ζ values in all the pH range considered. This is at variance with what observed by Colilla et al. who employed the same carboxyethylsilanetriol sodium salt to functionalize SBA-15 surface.[22] In their case the carboxy- sample showed a ζ potential curve similar to that of the parent SBA-15 material (same IEP), except for slightly more negative values in the 4.5-6.5 pH interval. In our case ζ became progressively more negative at increasing pH values, to reach -30 mV at pH 10. This suggests a high efficiency in the functionalization of MSN surface with the grafting agent and indicates that the carboxylate groups are only partially protonated even at the lowest pH values. Moreover, the similar ζ values of MSN and carboxy-MSN observed at pH 9-10 confirm the presence of residual Si-OH, which contributed to the overall negative charge.

3.2 Surface description: FTIR spectroscopy

Infrared spectroscopy was employed to get information on the surface sites present on the materials before and after functionalization. The spectra obtained on the three samples outgassed at RT are reported in Figure 4 in the high and low frequency ranges (top and bottom panels, respectively). In the latter only the spectra of the two functionalized samples are shown, since no information derives from MSN spectrum. The spectra were measured on self-supporting pellets with similar thickness (ca 5.5. mg/cm^2), so that a semi-quantitative comparison can be directly made.

The spectrum of MSN in the high frequency range is characterized by a sharp and intense band at 3744 cm^{-1}, with a shoulder at 3712 and a broad absorption centered at 3540 cm^{-1}. These modes are assigned to the Si-OH stretching modes (νSi-OH) of isolated and geminal, "terminal" (hydrogen bond acceptor) and "internal" (H-bond donor) silanol groups, respectively (Scheme 1).[43,78] The spectral shape is indicative of the surface species distribution and density, which are strongly influenced by silica origin (preparation route and calcination) and by resulting texture.[43, 44] In this case, the spectra are similar to those shown by "bulk" (that is not nanosized) mesoporous samples prepared by micelle template synthesis,[38, 43, 68, 69] for whom a silanol surface density of 4.5 OH/nm^2 was proposed in fair agreement with our TGA estimation.[41, 43] The corresponding spectrum of the reference material (Sipernat 320) is reported in Figure S3c for comparison. In this case a higher relative intensity of the bands related to hydrogen-bonded Si-OH with respect to isolated ones is observed, in agreement with the high surface density estimated by TGA.

Coming to the functionalized materials, the aminopropyl groups insertion is witnessed by: [58]i) appearance of signals at 3370/3306 and 2940/2870 cm^{-1} (due to $\nu_{as}/\nu_{sym}NH_2$ and ν_{as}/ν_{sym} CH_2 modes, respectively), ii) decrease of silanols bands at 3744 cm^{-1} and growing of a broad absorption related to H-bonding interactions in the 3700-2900 cm^{-1} range, iii) at low frequency (bottom panel of Figure 4) presence of the band at 1595 cm^{-1} (δNH_2 scissor vibration), with minor features between 1500 and 1350 cm^{-1} (δCH_2 modes). The two weak and broad components around 1640 and 1546 cm^{-1} (labelled with a star) were assigned to the δ_{as} modes of protonated NH_3^+ species.[58, 79] This assignment is in agreement with the occurrence of an acid-base reaction between amine functions and surface silanol groups resulting in ammoniumpropyl/silanolate couples (Scheme 2), as reported by different groups on aminopropyl-functionalized oxides.[76, 80, 81] On the other hand, the carboxylate groups insertion is witnessed by:[79, 82] i) appearance of signals between 3000 and 2850 cm^{-1} (assigned to carboxyethyl aliphatic νCH), ii) decrease of silanols signal at 3744 cm^{-1} and increase of νOH signals involved in H-bonding in the range 3700-2900 cm^{-1}, iii) at low frequency (Figure 4, bottom panel) formation of two intense bands at 1572 and 1418 cm^{-1} with a shoulder at 1400 cm^{-1} (assigned to COO^- ν_{as} and ν_{sym}, respectively). The higher intensity of these bands with respect to the 1595 cm^{-1} fingerprint of the amino groups is clearly related to a different extinction coefficient.

The infrared spectra of the three materials outgassed at RT and equilibrated with 1.5 mbar of water vapor are reported in Figure 5, in the high and low frequency region (top and bottom panels, respectively). This intermediate pressure was selected to better appreciate the position of the intense bands in the high frequency region (out of scale in the spectra obtained at the highest water coverage). However, for the sake of completeness a magnification of the isolated silanol region measured upon 9 mbar of water vapor (*i.e.* at the highest coverage examined) is reported in the inset of the corresponding figure. In all samples water adsorption was completely reversible by outgassing at the infrared beam temperature.

With respect to outgassed MSN spectrum (compare with Figure 4) water adsorption causes the consumption of both bands at 3744 and 3712 cm^{-1}, with the corresponding increase of a broad absorption centered at 3410 cm^{-1}, with components at 3665 and 3220 cm^{-1}, due to OH groups interacting via H-bonding with water molecules. More in detail, this broad absorption is due to the overlapping of the fundamental stretching vibrations (ν_1 and ν_3) of adsorbed water and to νSi-OH modes red-shifted by H-bonding interactions.[43] The isolated Si-OH groups are not totally consumed upon contact with 9 mbar of water vapor (see inset), in agreement with literature data reporting lower Brønsted acidity of isolated OH sites with respect to H-bonded or geminal ones.[37,40,43, 83] The corresponding spectrum in the low frequency range (Figure5, bottom panel) is characterized by the well-known bending mode of adsorbed water (δH_2O) at 1630 cm^{-1}.[40,43]

A similar behavior in the high frequency region (consumption of the band related to Si-OH groups and growth of a broad absorption related to H-bonded species) is observed on both the functionalized materials. Moreover, in the case of amino-MSN, the bands previously described and assigned to the two δ_{as} modes of protonated NH_3^+ species (1636 cm^{-1} - superimposed to the δH_2O at 1630 cm^{-1}- and 1546 cm^{-1}, bottom panel of Figure 5)[58, 79, 81] grow in intensity, suggesting an acid-base reaction in the presence of adsorbed water molecules. Clearly this proton transfer reaction involves only a small fraction of the aminopropyl groups, since the bands related to neutral amine (νNH_2 at 3370/3306 cm^{-1} and δNH_2 at 1595 cm^{-1}) are still present. A detailed investigation of this phenomenon will be the subject of a further publication. To the aim of this work, we can propose that the adsorption of water on the surface of amino-MSN mainly results in the formation of hydrogen bonded adducts with aminopropyl and silanol groups, as schematically depicted in Scheme 3.

Concerning the carboxy-MSN sample, water dosage results in the appearance in the low frequency range (Figure 5, bottom panel) of the typical δH_2O band of physisorbed water. This band is broader (FWHM 66 *vs* 41 cm^{-1}) and blue-shifted (1634 *vs* 1630 cm^{-1}) with respect to what observed on bare MSN, suggesting a more heterogeneous situation. Moreover, the COO^- ν_{as} and ν_{sym} modes of the functional groups are perturbed, in that the former moves from 1572 to 1562 cm^{-1}, and slightly increases in intensity, while the latter shows the relative growth of the component at 1404 cm^{-1}. Similar changes in the position of ν_{as} and ν_{sym} modes of carboxylate surfactants head-groups at the water-air and water-oil interface were related to the presence of hydrogen bonding interactions with water molecules.[84] The authors proposed a higher vibrational frequency for surfactants carboxylate head-groups less bonded to water, and a lower one for more water bound head-groups. These spectral changes are in agreement with what observed in this work, suggesting hydrogen-bonding interactions of water molecules with the oxygen atoms of the carboxylate groups. Noticeably, Beaman *et al.* proposed that each carboxylate group has four potential opportunities of forming H-bonds with nearby water, *i.e.* with two water molecules for each oxygen atom, although this extensive coordination could be limited by sterical hindrance.[84] Clearly, we cannot assume the same accessibility of carboxylate groups on the surface of carboxy-MSN, due to the curved pore surface and the presence of silanols. In Scheme 4, a hypothetical situation with three water molecules H-bonded to the carboxylate groups is depicted, with the sole aim to suggest the possibility of multiple (up to 3-4 water molecules per carboxylate group) interactions.

As reported in the literature,[43] infrared spectroscopy could be employed to estimate the amount of adsorbed water molecules by measuring the integrated intensity of the δH_2O band around 1630 cm^{-1}. Nevertheless, in the case of functionalized MSN samples this estimation was not possible due to the presence of overlapping bands (COO^- ν_{as} and δ_{as} of NH_3^+ groups).

3.3 Water adsorption microgravimetric measurements

3.3.1 Quantitative considerations

Water adsorption/desorption isotherms at 25, 35 and 50 °C nominal temperature were carried out on the three samples previously dehydrated at 50°C for 6 hours. The activation conditions were selected on the basis of infrared evidences, showing the removal of physisorbed water after prolonged outgassing at RT. Moreover, the sample weight was found to be stable after 2-3 hours outgassing at this temperature. Water sorption experiments were repeated twice for each temperature, to evaluate the occurrence of irreversible phenomena. Data were very similar for the two runs, at least within the experimental uncertainty (Figure S4), confirming the infrared observation that water adsorption is a reversible process and no dissociative phenomena occur. For simplicity only the secondary desorption isotherm data were fitted with a spline function and reported in the following.

The results obtained on MSN sample at the three temperatures (expressed as $\mu mol/m^2$ for a direct comparison with the literature) are reported in Figure 6; readers can refer to Figures S5 and S6 for the same experiments carried out on the functionalized samples and reference Sipernat 320, respectively. For all samples the water uptakes measured at an equilibrium vapor pressure of 9 mbar are resumed in Table 2.

The reference sample Sipernat 320 is a precipitated silica and was selected as a supposedly hydrophilic material.[37, 85] This assumption was confirmed by the high water uptake measured in this work (16.2 µmol/m^2 at 25 °C and 9 mbar, see Table 2), as compared to other reports on hydrophilic silica materials.[37, 48] For instance, Bolis et al. compared hydrophilic and hydrophobic silica-based samples (quartz and different amorphous silica, both precipitated and pyrogenic) and found a maximum water uptake at RT and 5 mbar of 7-8 µmol/m^2 on the hydrophilic ones.[37] In similar conditions a water uptake of *ca* 13 µmol/m^2 was measured in this work on Sipernat 320 (Figure S6). Bocian et al. measured a maximum water uptake around 18 µmol/m^2 on polar silica hydride stationary phases.[48] The high water uptake of the reference material is in agreement with the high surface OH density measured by TGA and observed by infrared spectroscopy (see above and Figure S3c).

The water uptake of bare MSN at the three temperatures is definitely smaller with respect to what measured in the same conditions on the reference Sipernat 320 material. The value measured at 25 °C is instead quite similar to what reported by Cauvel et al. (*ca* 4.5 µmol/m^2 at 9 mbar),[38] who carried out gasvolumetric water adsorption experiments at RT on a "bulk" micelle template mesoporous silica. Noticeably, these values are close to what reported for hydrophobic pyrogenic silica,[86] as pointed out by Cauvel et al.[38]

The effect of surface functionalization on water uptake was analyzed by comparing the results obtained on the three MSN materials at 35 °C (Figure 7). The temperature was chosen as it is similar to the one estimated on the pellet exposed to the infrared beam. In this case the uptake data are reported as mmol of water adsorbed for gram of sample. The problem concerning the data presentation in the case of surface modified silicas deserves some consideration. In fact, the usual comparison of the adsorption capacity of materials with different textural properties is made by normalizing the adsorbent uptake to the sample SSA[37, 38] (as done in Figure 6 and Table 2, column 2-4). However, in the present work, the differences measured by nitrogen adsorption experiments on the three samples (Table 1) are not related to really different textural properties but to the lining of the pores caused by the grafting agent. Thus, this procedure should cause an overestimation of the real adsorbing properties of modified materials (see Figure S7, where the data expressed as $\mu mol/m^2$ are compared for the three MSN materials). To avoid this problem Brunel at al.[68] reported water adsorption data normalized with respect to the mass of silica, *i.e.* excluding the contribution of functionalizing groups. This approach was reasonable since the grafted species were alkyl chains, unlikely to give H-bonding interactions with water, but the same is less acceptable in the case of amino and carboxylate groups. Notwithstanding these difficulties, the results clearly show that, from the quantitative point of view, grafting with sodium ethylcarboxylate groups causes a large increase in the adsorption capacity of MSN. On the contrary aminopropyl functionalization has a very mild effect on this parameter.

3.3.2 Isosteric heat of adsorption calculation

Water isosteric heat of adsorption (q_{st}) of the three MSN samples and reference material was calculated by employing the Clausius-Clapeyron equation (eq. 1), that is by a plot of lnp *vs* 1/T at fixed coverage (*i.e*. water uptake). q_{st} can be related to q_{ads}, which is the heat directly measured in a calorimeter for an incremental dose of gas (Δm) introduced at the temperature of the cell, through the equation:[87-90]

$$-q_{ads} = \frac{Q+V\Delta p}{\Delta m} \qquad (2)$$

where V is the dead space in the sample cell. The term $V\Delta p$ in eq. (2) is usually small compared to Q. Since adsorption is exothermic, Q is negative. In the literature, q_{ads} is often referred to as q_{diff}, which is the differential heat of adsorption measured in a calorimeter defined as heat evolution when unit adsorption takes place. This implies that q_{diff} should be obtained point by point from the ratio dQ/dm, whereas it is actually obtained dose by dose from the ratio ΔQ/Δm.

q_{ads} can be directly related to the adsorption enthalpy, by assuming ideal gas conditions:[87-90]

$$q_{ads} = -\Delta H \qquad (3)$$

Since q_{st} calculated by the Clausius-Clapeyron equation is comparable to the q_{ads} measured in a microcalorimeter,[88] eq. (3) implies that the former can be compared to the latent enthalpy of water liquefaction (q_L = 44 kJ/mol). Surfaces evolving adsorption heats higher than q_L are defined as hydrophilic, whereas values lower than q_L implies hydrophobic surfaces.[38, 45]

In this work the consistency of the experimental approach was checked by comparing the average q_{st} value ($\bar{q}_{st}$) calculated for the reference sample Sipernat 320 (Figure S6 and Table 2) with q_{ads} directly measured by microcalorimetry (Figure S3d). Average q_{ads} ($\bar{q}_{ads}$) measured above 1 mmol/g (a water uptake interval comparable to the microgravimetric measurements, see below) is 65 ± 2 kJ/mol, in good agreement with the calculated $\bar{q}_{st}$ value of 59 ± 3 kJ/mol.

The experimental microgravimetric data reported in Figures 6 (MSN), S5 (amino- and carboxy-MSN) and S6 (Sipernat 320) were employed for calculation of q_{st} after interpolation with cubic spline curves. The horizontal segments in the figures represent the isosters selected for the calculation. From the figures it can be seen that only few of the isosters are likely to give reliable T and p values, due to the lack of experimental points at low coverage (water uptake minor than 1 mmol/g). To avoid this problem, and to check the consistency of the data, additional adsorption experiments were carried out on the three samples in different pressure ranges and/or different temperatures (21, 31 and 40 °C, Figure S8). The calculated q_{st} data are reported in Figure 8 (Figure S6 for the reference Sipernat 320 sample) as a function of water uptake N_{ads}. The changes of q_{st} *vs* N_{ads} are likely due to the experimental error connected to the employed methodology, so that only the average $\bar{q}_{st}$ values summarized in Table 2 will be employed to compare the surface features of the different materials.

All the $\bar{q}_{st}$ values reported in Table 2 are higher than q_L, indicating that all samples can be classified as hydrophilic. The value calculated for MSN ($\bar{q}_{st}$ = 51 ± 3 kJ/mol) is smaller with respect to the two functionalized samples, which show values similar within the experimental error (61 ± 4 and 65 ± 3 kJ/mol for amino- and carboxy-MSN, respectively) and comparable to what measured for reference Sipernat 320 sample (59 ± 3 kJ/mol).

3.4. Discussion

The qualitative and quantitative results described above can be discussed by considering the mechanisms controlling water interaction at the surface of silica. It is well ascertained that hydrophobic surfaces (q_{st} < 44 kJ/mol) are characterized by the main presence of isolated silanols, which can give only one H-bond with one water molecule.[37, 68, 86, 91, 92] On the contrary, the hydrophilic character (q_{st} > 44 kJ/mol) can be related to the presence of hydroxyl-rich surfaces, where each water molecule can be hydrogen-bonded to two silanols, and each silanol can interact with two water molecules.[37, 38, 93, 94]

The silanol density and distribution, which can be estimated by TGA (Figure 2) and monitored by infrared spectroscopy (Figures 4 and S3c), respectively, are thus the main parameters affecting both adsorption heat and water uptake. On the basis of what discussed above, it is clear that these two factors are usually related, so that hydrophilic surfaces usually also show high water uptakes. This was indeed observed in this work on the reference Sipernat 320 material, which showed: i) high surface OH density (15.1 OH/nm^2); ii) an infrared spectrum rich in H-bonded silanols (compare the intensity of the broad band at 3469 with the one at 3737 cm^{-1} in Figure S3c); iii) high $\bar{q}_{ads}$ and $\bar{q}_{st}$ values (65 ± 2 and 59 ± 3 kJ/mol, respectively); iv) high water uptakes (16.2 μmol/m^2 at 25 °C and 9 mbar).

The data obtained on the MSN prepared and characterized in this work are however more controversial. The estimated silanol density (3.3 OH/nm^2) is in agreement with the infrared spectrum showing a relatively high amount of isolated Si-OH groups (band at 3744 cm^{-1} in Figure 4). However, the calculated $\bar{q}_{st}$ value (51 ± 3 kJ/mol) indicates a hydrophilic surface, in contrast with the low water uptake, which is similar to what measured on hydrophobic pyrogenic silica.[86] A similar discrepancy was observed by Cauvel et al. on the already mentioned micelle-templated mesoporous silica: q_{ads} around 60 kJ/mol and water uptake of 4.3 $\mu mol/m^2$ at 9 mbar and 25 °C.[38] The authors explained these data by hypothesizing a heterogeneous distribution of surface Si-OH groups. Namely, they proposed the presence of patches of hydroxyl-rich regions (showing the predominance of H-bonded species, as in Schemes 1b,c) alternating with hydroxyl-poor ones (showing mainly the isolated groups depicted in Scheme 1a).[68] We can thus put forward the hypothesis that this peculiar feature is intrinsic of the porous structure, since it is observed in this work on a nanosized material prepared by a different synthetic procedure.

Coming to the functionalized materials, both showed a consistent increase in the calculated $\bar{q}_{st}$ values, indicating an increase in the surface hydrophilicity. The differences between the two values for amino- and carboxy-MSN are within the experimental error (61 ± 4 *vs* 65 ± 3 kJ/mol, respectively), so that they cannot account for the completely different water uptake. The results obtained on the two samples will be thus discussed separately.

In the case of amino-MSN, infrared spectroscopy of dehydrated sample showed the presence of aminopropyl groups, silanols and a small amount of protonated ammoniumpropyl species[76, 80] (Figure 4 and Scheme 2). By comparing the spectrum of dehydrated amino-MSN with parent MSN, we can infer that a large amount of H-bonding silanol groups (band at 3540 cm^{-1}) were consumed by grafting with the alkoxysilane, so that for simplicity we will assume that unreacted silanols are mainly isolated, as depicted in Schemes 1 and 2. This is only a simplifying assumption for the sake of pictorial representation (Scheme 2), since we cannot exclude that some patches of hydrogen-bonded Si-OH groups, inside the pores, were unaffected by the post-synthesis procedure due to alkoxysilane diffusion issues. All these surface species are likely to interact by H-bonding with water molecules, even if, for simplicity, in Scheme 2 only the interactions taking place with neutral entities are represented. The formation of ammoniumpropyl groups upon water interaction (testified by the growth of the bands at 1636 and 1546 cm^{-1} in Figure 5) will be the subject of further investigations. For the scope of this paper, it is sufficient to mention the fact that this phenomenon affects only a small fraction of the aminopropyl grafted groups, so that quantitative data can be discussed mainly considering the H-bonded species represented in Scheme 3. However, it is important to mention here the results reported by Calvo et al. on aminopropyl functionalized mesoporus silica films. The authors showed the protonation of a fraction of amino groups as a function of pH, and proposed an acid-base equilibrium between $–NH_3^+$ and SiO^- groups, which could be influenced by the presence of water molecules.[81]

When one compares the $\bar{q}_{st}$ values of amino-MSN with the one calculated for parent MSN, a consisted increase is observed (61 ± 4 *vs* 51 ± 3 kJ/mol, last column of Table 2), which does not correspond to a large increase in water uptake. This suggests that the higher calculated adsorption heat is due to species strongly interacting with water molecules, *i.e.* amino groups showing higher basicity with respect to silanols. A precise quantification of the water/amino interaction at the surface of functionalizes silica is unfortunately not possible, since the calculated values also average H-bonding interactions with silanols, as indicated by infrared spectroscopy (inset of Figure 5).

In analogy to what described above for amino-MSN, we can described the surface of carboxy-MSN samples as mainly exposing ethylcarboxylate groups and isolated silanols. These are thus the species involved in H-bonding interactions with water, resulting in a $\bar{q}_{st}$ value of 65 ± 3 kJ/mol and a water uptake sensibly higher with respect to parent MSN. This suggests that also in this case H-bonding interactions with grafted groups are stronger with respect to the ones taking place with silanols. Moreover, the high water uptake can be ascribed to the possibility of multiple (two or three) H-bonding interactions of water molecules with the carboxylate anion, as depicted in Scheme 4.

4. Conclusions

This work deals with the synthesis and physico-chemical characterization of mesoporous silica nanoparticles (MSN), as prepared and functionalized with two different grafting agents: aminopropyl and sodium ethylcarboxylate groups. Different techniques (TEM, XRD, nitrogen adsorption/desorption isotherms) confirmed that the samples are characterized by nanosized morphology with a MCM-41 like regular array of cylindrical pores. These features are preserved after functionalization, which causes a definite change in the exposed surface groups (as evidenced by infrared spectroscopy) and in the surface charge of the materials (as monitored by ζ potential measurements). These properties make the prepared systems potential nanocarriers for the adsorption and delivery of drugs or bioactive molecules in physiological fluids, as described elsewhere.[95, 96]

Due to the application field, and to the importance of surface properties in affecting nanoparticles fate in biological and environmental conditions,[23, 30, 31] attention was focused on the determination of the samples hydrophilic character. This was obtained by quantitative microgravimetric measurements which allowed the calculation of the average isosteric heat of adsorption $\bar{q}_{st}$. The results indicate that all samples are hydrophilic, showing $\bar{q}_{st}$ values higher than the latent enthalpy of water liquefaction (q_L = 44 kJ/mol).

However, markedly higher $\bar{q}_{st}$ values were measured for the two functionalized materials, indicating a positive effect of surface functionalization on hydrophilicity. This is related to specific interactions of water molecules with the two functional groups. Moreover, coupling these data with infrared evidences and measured water uptakes allowed to propose a molecular description of the main H-bonding interactions taking place in the presence of water. Namely, one-to-one water/amino adducts were proposed on the aminopropyl functionalized materials, while the formation of multiple H-bonding interactions (involving two or three water molecules) with ethylcarboxylate anions was proposed.

These findings can be useful to describe the MSNs *in vivo* complex ensemble of processes and phenomena occurring at the material surface and mediated by the presence of water adsorbed molecules. For instance, the crucial impact of surface functionalization on the blood compatibility of MSNs was reported. In fact, the authors pointed out that the interactions between MSNs and blood constituents are not simply dependent on the surface charge of the nanoparticles but seem to be affected by the chemical composition of the surface functional groups.[33]

The results described in this work could be also discussed in view of the very interesting findings by Calvo et al.,[81] as already mentioned. The authors developed hybrid mesoporous aminopropyl-functionalized thin films and studied the influence of pH and of inorganic moieties (Si, Ti or Zr oxides) on the speciation of amino/ammonium groups at the external and inner surface of the mesoporous films. More in detail, XPS analysis allowed to quantify the ratio R between ammonium and amino groups on samples submitted to a given pH, allowing to assess the materials IEP and the aminopropyl group pK_a. These results show that the pH dependence of R depends on the chemical nature of the metal oxide, and that the R value changes in a broader pH range with respect to ammonium/amine equilibrium in solution. These aspects were explained by considering the acid/base interactions taking place at the surface of organo-inorganic thin films, suggesting that $–NH_3^+$ groups near SiO^- groups are unstable, leading to $–NH_2$ and Si-OH couples.

As pointed out by the authors, the role of solvation on this acid/base equilibrium is an important aspect deserving to be further studied. Our results clearly confirm a specificity in the water interaction with surface groups on amino- and carboxylate functionalized MSN, and allows an estimation of the corresponding energetics. This represents a small step in the rationalization of this complex topic, helping to understand the water-mediated reactivity of functional surface groups towards biomolecules, and their role in perm-selectivity.

Acknowledgements

We thank Dr I. Miletto for help and inspiration. Prof. L. Marchese and Dr. G. Paul from Università del Piemonte Orientale ‘‘A. Avogadro” are gratefully acknowledged for fruitful discussions. Compagnia di San Paolo and University of Turin are gratefully acknowledged for funding Project ORTO114XNH through ‘‘Bando per ilfinanziamento di progetti di ricerca di Ateneo - anno 2011. This work was supported by the European COST Action MP1202 “Rational design of hybrid organic inorganic interfaces: the next step towards advanced functional materials”.

References

1. M. Vallet-Regí, A. Rámila, R. P. del Real and J. Pérez-Pariente, *Chem. Mater*, 2001, **13**, 308−311.
2. M. Vallet-Regí, F. Balas and D. Arcos, *Angew. Chem. Int. Edit.*, 2007, **46**, 7548-7558.
3. M. W. Ambrogio, C. R. Thomas, Y.-L. Zhao, J. I. Zink and J. F. Stoddart, *Acc. Chem. Res.*, 2011, **44**, 903-913.
4. T. Fontecave, C. Sanchez, T. Azais and C. Boissiere, *Chem. Mater.*, 2012, **24**, 4326-4336.
5. J. M. Rosenholm, C. Sahlgren and M. Linden, *Nanoscale*, 2010, **2**, 1870-1883.
6. S. Wang, *Microporous Mesoporous Mater.*, 2009, **117**, 1-9.
7. Z. Li, J. C. Barnes, A. Bosoy, J. F. Stoddart and J. I. Zink, *Chem. Soc. Rev.*, 2012, **41**, 2590-2605.
8. WO2014120922-A1, 2014.
9. J. Andersson, J. Rosenholm, S. Areva and M. Linden, *Chem. Mater.*, 2004, **16**, 4160 – 4167.
10. R. Mellaerts, E. J. Fayad, G. Van den Mooter, P. Augustijns, M. Rivallan, F. Thibault-Starzyk and J. A. Martens, *Mol. Pharm.*, 2013, **10**, 567-573.
11. D. R. Radu, C. Y. Lai, K. Jeftinija, E. W. Rowe, S. Jeftinija and V. S. Y. Lin, *J. Am. Chem. Soc.*, 2004, **126**, 13216-13217.
12. I. I. Slowing, J. L. Vivero-Escoto, C.-W. Wu and V. S. Y. Lin, *Adv. Drug Deliv. Rev.*, 2008, **60**, 1278-1288.
13. S.-H. Wu, Y. Hung and C.-Y. Mou, *Chem. Commun.*, 2011, **47**, 9972-9985.
14. D. J. Irvine, *Nat. Mater.*, 2011, **10**, 342-343.
15. F. Tang, L. Li and D. Chen, *Adv. Mater.*, 2012, **24**, 1504-1534.
16. X. Huang, X. Teng, D. Chen, F. Tang and J. He, *Biomaterials*, 2010, **31**, 438-448.
17. F. Lu, S. Wu and C. Mou, *Small*, 2009, **5**, 1408-1413.
18. M. Manzano, M. Colilla and M. Vallet-Regí, *Expert Opin. Drug Deliv.*, 2009, **6**, 1383-1400.
19. J. M. Rosenholm and M. Linden, *J. Control. Release*, 2008, **128**, 157-164.
20. D. P. Ferris, J. Lu, C. Gothard, R. Yanes, C. R. Thomas, J.-C. Olsen, J. F. Stoddart, F. Tamanoi and J. I. Zink, *Small*, 2011, **7**, 1816-1826.
21. J. M. Rosenholm, E. Peuhu, J. E. Eriksson, C. Sahlgren and M. Linden, *Nano Lett.*, 2009, **9**, 3308-3311.
22. M. Colilla, I. Izquierdo-Barba, S. Sanchez-Salcedo, J. L. G. Fierro, J. L. Hueso and M. Vallet-Regí, *Chem. Mater.*, 2010, **22**, 6459-6466.
23. S. T. Kim, K. Saha, C. Kim and V. M. Rotello, *Acc. Chem. Res.*, 2013, **46**, 681-691.

24. H. Meng, M. Xue, J. I. Zink and A. E. Nel, *J. Phys. Chem. Lett.*, 2012, **3**, 358-359.
25. H. Meng, M. Liong, T. Xia, Z. Li, Z. Ji, J. I. Zink and A. E. Nel, *ACS Nano*, 2010, **4**, 4539-4550.
26. Y.-S. Lin, N. Abadeer and C. L. Haynes, *Chem. Commun.*, 2011, **47**, 532-534.
27. X. Huang, J. Zhuang, X. Teng, L. Li, D. Chen, X. Yan and F. Tang, *Biomaterials*, 2010, **31**, 6142-6153.
28. M. Zhu, G. Nie, H. Meng, T. Xia, A. Nel and Y. Zhao, *Acc. Chem. Res.*, 2013, **46**, 622-631.
29. Y.-S. Lin and C. L. Haynes, *J. Am. Chem. Soc.*, 2010, **132**, 4834-4842.
30. Z. Tao, B. B. Toms, J. Goodisman and T. Asefa, *Chem. Res. Toxicol.*, 2009, **22**, 1869-1880.
31. J. L. Townson, Y.-S. Lin, J. O. Agola, E. C. Carnes, H. S. Leong, J. D. Lewis, C. L. Haynes and C. J. Brinker, *J. Am. Chem. Soc.*, 2013, **135**, 16030-16033.
32. Z. Ma, J. Bai, Y. Wang and X. Jiang, *ACS Appl. Mater. Interfaces*, 2014, **6**, 2431-2438.
33. A. Yildirim, E. Ozgur and M. Bayindir, *Journal of Materials Chemistry B*, 2013, **1**, 1909-1920.
34. D. G. Castner and B. D. Ratner, *Surf. Sci.*, 2002, **500**, 28-60.
35. B. Kasemo, *Surf. Sci.*, 2002, **500**, 656-677.
36. L. Bertinetti, A. Tampieri, E. Landi, C. Ducati, P. A. Midgley, S. Coluccia and G. Martra, *J. Phys. Chem. C*, 2007, **111**, 4027-4035.
37. V. Bolis, B. Fubini, L. Marchese, G. Martra and D. Costa, *J. Chem. Soc., Faraday Trans.*, 1991, **87**, 497-505.
38. A. Cauvel, D. Brunel, F. DiRenzo, E. Garrone and B. Fubini, *Langmuir*, 1997, **13**, 2773-2778.
39. Y. I. Tarasevich, V. E. Polyakov, A. A. Serdan and G. V. Lisichkin, *Colloid J.*, 2005, **67**, 638-643.
40. M. Takeuchi, L. Bertinetti, G. Martra, S. Coluccia and M. Anpo, *Appl. Catal. A-Gen.*, 2006, **307**, 13-20.
41. P. Ugliengo, M. Sodupe, F. Musso, I. J. Bush, R. Orlando and R. Dovesi, *Adv. Mater.*, 2008, **20**, 4579-4583.
42. J. Pires, M. Pinto, J. Estella and J. C. Echeverria, *J. Colloid Interface Sci.*, 2008, **317**, 206-213.
43. J. P. Gallas, J. M. Goupil, A. Vimont, J. C. Lavalley, B. Gil, J. P. Gilson and O. Miserque, *Langmuir*, 2009, **25**, 5825-5834.
44. S. A. Kozlova and S. D. Kirik, *Microporous Mesoporous Mater.*, 2010, **133**, 124-133.

45. M. Thommes, J. Morell, K. A. Cychosz and M. Froeba, *Langmuir*, 2013, **29**, 14893-14902.

46. C. Chen, S. Shi, M. Wang, H. Ma, L. Zhou and J. Xu, *J. Mater. Chem. A*, 2014, **2**, 8126-8134.

47. B. Torun, C. Kunze, C. Zhang, T. D. Kuehne and G. Grundmeier, *Phys. Chem. Chem. Phys.*, 2014, **16**, 7377-7384.

48. S. Bocian, G. Rychlicki, M. Matyska, J. Pesek and B. Buszewski, *J. Colloid Interface Sci.*, 2014, **416**, 161-166.

49. S. A. Mian, L.-M. Yang, L. C. Saha, E. Ahmed, M. Ajmal and E. Ganz, *Langmuir*, 2014, **30**, 6906-6914.

50. K. H. Nielsen, T. Kittel, K. Wondraczek and L. Wondraczek, *Scientific Reports*, 2014, **4**.

51. R. Lin, J. Liu, Y. Nan, D. W. DePaoli and L. L. Tavlarides, *Ind. Eng. Chem. Res.*, 2014, **53**, 16015-16024.

52. D. Hou, H. Ma, Z. Li and Z. Jin, *Acta Mater.*, 2014, **80**, 264-277.

53. M. Boudot, D. R. Ceratti, M. Faustini, C. Boissiere and D. Grosso, *J. Phys. Chem. C*, 2014, **118**, 23907-23917.

54. P. Gomez-Alvarez and S. Calero, *Crystengcomm*, 2015, **17**, 412-421.

55. D. Tarn, M. Xue and J. I. Zink, *Inorg. Chem.*, 2013, **52**, 2044-2049.

56. G. T. Hermanson, *Bioconjugate Techniques*, Academic Press2008.

57. L. Wang, W. Zhao, M. B. O'Donoghue and W. Tan, *Bioconjugate Chem.*, 2007, **18**, 297-301.

58. P. Iliade, I. Miletto, S. Coluccia and G. Berlier, *Res. Chem. Intermed.*, 2012, **38**, 785-794.

59. M. Kruk, M. Jaroniec, Y. Sakamoto, O. Terasaki, R. Ryoo and C. H. Ko, *J. Phys. Chem. B*, 2000, **104**, 292-301.

60. M. Schoeffel, N. Brodie-Linder, F. Audonnet and C. Alba-Simionesco, *J. Mater. Chem.*, 2012, **22**, 557-567.

61. R. J. Hunter, *Zeta potential in colloid science. Principles and applications.*, Academic Press, London, 1988.

62. X. S. Zhao, G. Q. Lu, A. K. Whittaker, G. J. Millar and H. Y. Zhu, *J. Phys. Chem. B*, 1997, **101**, 6525-6531.

63. C. Despas, A. Walcarius and J. Bessiere, *Langmuir*, 1999, **15**, 3186-3196.

64. B. H. Wouters, T. H. Chen, M. Dewilde and P. J. Grobet, *Microporous Mesoporous Mater.*, 2001, **44**, 453-457.

65. G. Hartmeyer, C. Marichal, B. Lebeau, S. Rigolet, P. Caullet and J. Hernandez, *J. Phys. Chem. C*, 2007, **111**, 9066-9071.

66. A. Salis, D. F. Parsons, M. Bostrom, L. Medda, B. Barse, B. W. Ninham and M. Monduzzi, *Langmuir*, 2010, **26**, 2484-2490.

67. B. Prelot, S. Lantenois, Y. Nedellec, M. Lindheimer, J.-M. Douillard and J. Zajac, *Colloid Surf. A*, 2010, **355**, 67-74.

68. D. Brunel, A. Cauvel, F. Di Renzo, F. Fajula, B. Fubini, B. Onida and E. Garrone, *New J. Chem.*, 2000, **24**, 807-813.

69. T. Martin, A. Galarneau, F. Di Renzo, F. Fajula and D. Plee, *Angew. Chem. Int. Edit.*, 2002, **41**, 2590-2592.

70. M. Jaroniec, C. P. Jaroniec, M. Kruk and R. Ryoo, *Adsorption*, 1999, **5**, 313-317.

71. K. C. Vrancken, P. Vandervoort, I. Gillisdhamers, E. F. Vansant and P. Grobet, *J. Chem. Soc., Faraday Trans.*, 1992, **88**, 3197-3200.

72. K. C. Vrancken, L. Decoster, P. Vandervoort, P. J. Grobet and E. F. Vansant, *J. Colloid Interface Sci.*, 1995, **170**, 71-77.

73. M. Etienne and A. Walcarius, *Talanta*, 2003, **59**, 1173-1188.

74. X. Rios, P. Moriones, J. C. Echeverria, A. Luquin, M. Laguna and J. J. Garrido, *Adsorption*, 2011, **17**, 583-593.

75. C. Giaveno, L. Celi, R. M. Aveiro Cessa, M. Prati, E. Bonifacio and E. Barberis, *Soil Sci.*, 2008, **173**, 694-706.

76. A. Walcarius, M. Etienne and B. Lebeau, *Chem. Mater.*, 2003, **15**, 2161-2173.

77. J. M. Waller and H. I. Maibach, *Skin Research and Technology*, 2005, **11**, 221–235.

78. F. Musso, M. Sodupe, M. Corno and P. Ugliengo, *J. Phys. Chem. C*, 2009, **113**, 17876-17884.

79. G. Socrates, *Infrared and Raman characteristic group frequencies*, John Wiley & Sons Ltd, Chichester, England, 2006.

80. A. Walcarius, M. Etienne and J. Bessiere, *Chem. Mater.*, 2002, **14**, 2757-2766.

81. A. Calvo, P. C. Angelome, V. M. Sanehez, D. A. Scherlis, F. J. Williams and G. J. A. A. Soler-Illia, *Chem. Mater.*, 2008, **20**, 4661-4668.

82. S. Fiorilli, B. Onida, B. Bonelli and E. Garrone, *J. Phys. Chem. B*, 2005, **109**, 16725-16729.

83. M. Delle Piane, M. Corno, A. Pedone, R. Dovesi and P. Ugliengo, *J. Phys. Chem. C*, 2014, **118**, 26737-26749.

84. D. K. Beaman, E. J. Robertson and G. L. Richmond, *J. Phys. Chem. C*, 2011, **115**, 12508-12516.

85. V. Bolis, A. Cavenago and B. Fubini, *Langmuir*, 1997, **13**, 895-902.

86. B. Fubini, V. Bolis, A. Cavenago, E. Garrone and P. Ugliengo, *Langmuir*, 1993, **9**, 2712-2720.
87. F. Siperstein, R. J. Gorte and A. L. Myers, *Langmuir*, 1999, **15**, 1570-1576.
88. D. M. Shen, M. Bulow, F. Siperstein, M. Engelhard and A. L. Myers, *Adsorption*, 2000, **6**, 275-286.
89. R. M. A. Roque-Malherbe, *Adsorption and Diffusion in Nanoporous Materials*, CRC Press, Taylor & Francis Group, Boca Raton (FL), 2007.
90. V. J. Inglezakis and A. A. Zorpas, *Desalination and Water Treatment*, 2012, **39**, 149-157.
91. V. Bolis, G. Magnacca, G. Cerrato and C. Morterra, *Langmuir*, 1997, **13**, 888-894.
92. S. Tosoni, B. Civalleri and P. Ugliengo, *J. Phys. Chem. C*, 2010, **114**, 19984-19992.
93. V. Bolis, C. Busco, S. Bordiga, P. Ugliengo, C. Lamberti and A. Zecchina, *Appl. Surf. Sci.*, 2002, **196**, 56-70.
94. F. Musso, P. Mignon, P. Ugliengo and M. Sodupe, *Phys. Chem. Chem. Phys.*, 2012, **14**, 10507-10514.
95. I. Miletto, A. Massa, E. Ugazio, G. Musso, G. Caputo and G. Berlier, *Phys. Chem. Chem. Phys.*, 2014, **16**, 12172-12177.
96. S. Sapino, E. Ugazio, L. Gastaldi, I. Miletto, B. G., D. Zonari and S. Oliaro-Bosso, *Eur. J. Pharm. Biopharm.*, 2015, **89**, 116–125.

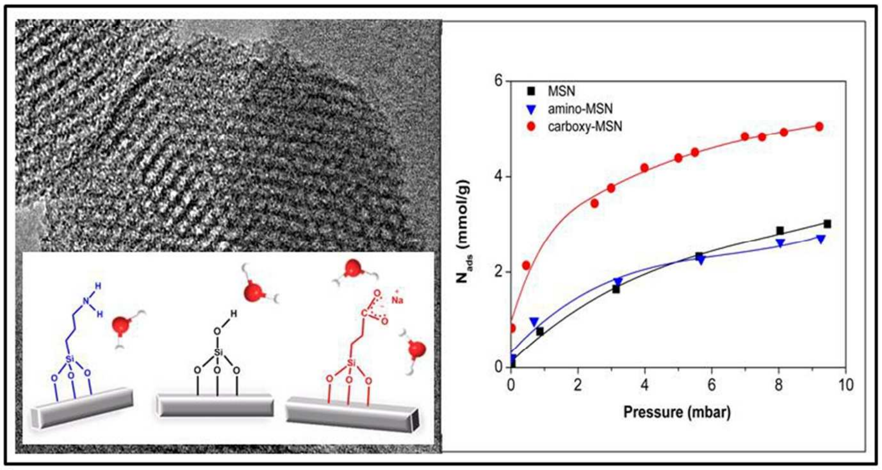

Microgravimetric water sorption isotherms measured on functionalized mesoporous silica nanoparticles (MSN)
254x190mm (96 x 96 DPI)

Table 1 General properties of the studied materials

Samples	SSA	Pore diameter	Pore volume	d_{100}	Wall Thickness	Functional group/nm^2	
	(m^2·g^{-1})	(Å)	(cm^3·g^{-1})	(Å)	(Å)	TGA	CHN
MSN	1090	35	1.35	37.7	8.6	-	-
amino-MSN	751	31	0.74	37.2	13.0	0.90	0.73
carboxy-MSN	845	31	0.80	35.8	10.3	0.40	0.46
Sipernat 320	173	~500	0.95	-	-	-	-

Table 2 Water uptake at 9 mbar and average isosteric molar heat of adsorption of the three MSN and a reference hydrophilic material for comparison

Samples	n_{ads} µmol/m^2			n_{ads} mmol/g			kJ/mol
	25°C	35°C	50°C	25°C	35°C	50°C	
MSN	4.3	2.7	1.5	4.7	3.0	1.6	51 ± 3
amino-MSN	5.1	3.6	2.1	3.7	2.7	1.6	61 ± 4
carboxy-MSN	7.1	6.3	4.4	6.4	5.0	4.0	65 ± 3
Sipernat 320	16.2	13.6	9.0	2.8	2.3	1.6	59 ± 3

Figure captions

Figure 1. HRTEM images of MSNs.

Figure 2. TGA profiles of a) MSN, b) amino-MSN and c) carboxy-MSN.

Figure 3. Zeta potential (ζ) curves as a function of pH at constant ionic strength for MSN (■), amino-MSN (▲) and carboxy-MSN (●).

Figure 4. Infrared spectra in the high (top) and low (bottom) frequency ranges of RT dehydrated a) MSN, b) amino-MSN and c) carboxy-MSN.

Figure 5. Infrared spectra in the high (top) and low (bottom) frequency ranges of samples outgassed at RT and contacted with 1.5 mbar water vapor: a) MSN, b) amino-MSN and c) carboxy-MSN. The inset of top panel reports the spectra recorded upon contact with 9 mbar of water vapor.

Figure 6. Water desorption microgravimetric isotherms measured on sample MSN at 25.2 (□), 35.0 (Δ) and 49.2 °C (○). The experimental data were fitted with cubic spline curves. Horizontal segments represent the isosters employed for the estimation of q_{st}.

Figure 7. Water desorption microgravimetric isotherms measured at the nominal temperature of 35 °C on MSN (■), amino-MSN (▼) and carboxy-MSN (●).

Figure 8. Isosteric heat of adsorption versus water uptake for MSN (■), amino-MSN (▼) and carboxy-MSN (●). q_L = 44 kJ/mol (latent enthalpy of water liquefaction).

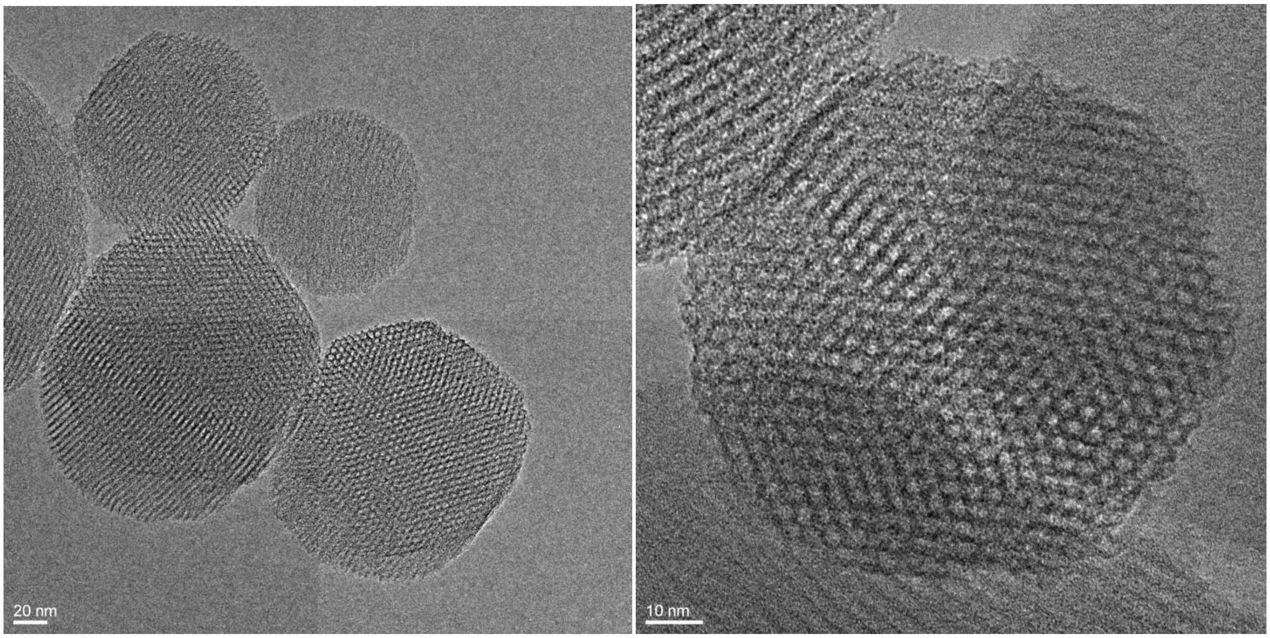

Figure 1

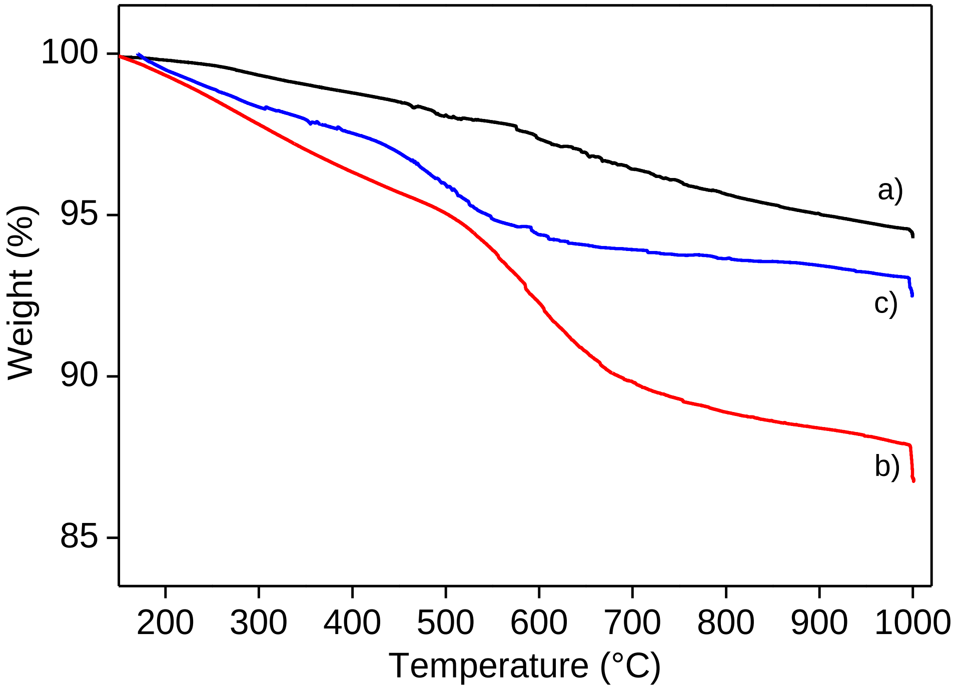
100
95
90
85
Weight (%)
200
300
400
500
600
700
800
900
1000
Temperature (°C)
a)
c)
b)

Figure 2

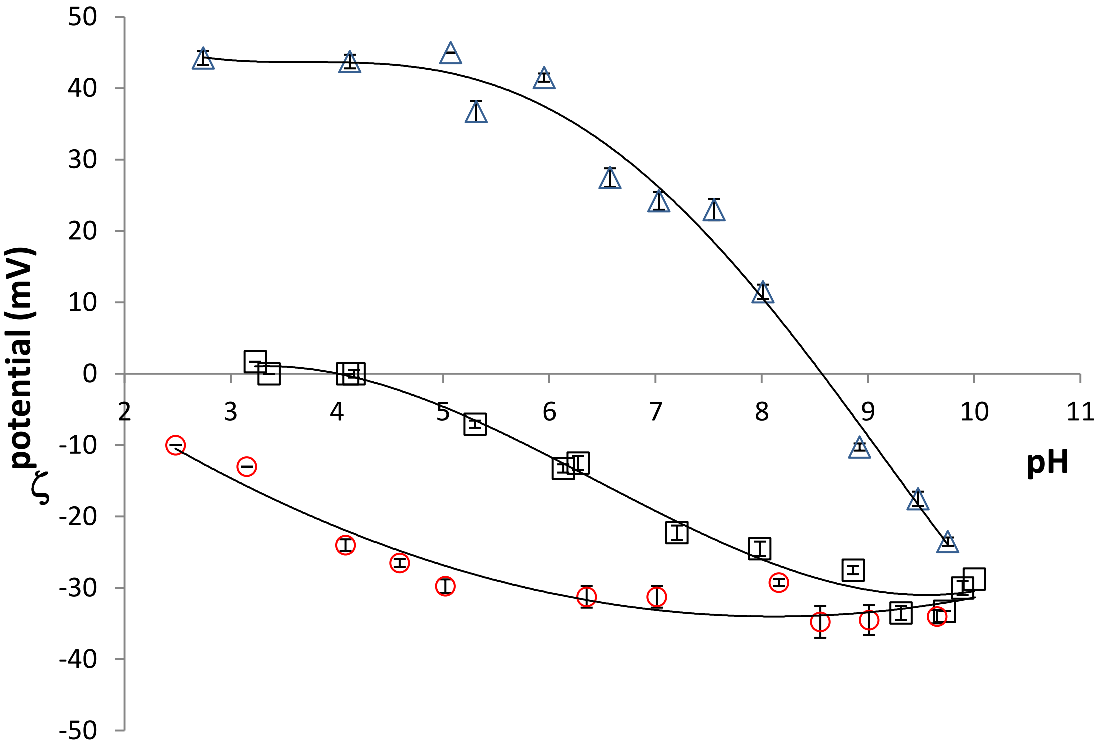

Figure 3

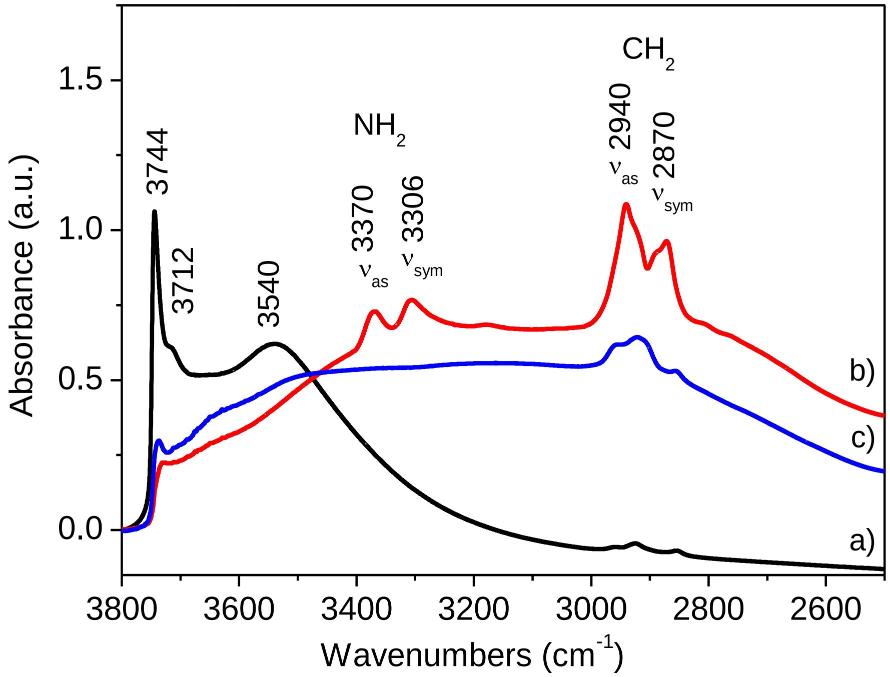
Absorbance (a.u.)
Wavenumbers (cm-1)
3744
3712
3540
NH2
3370 νas
3306 νsym
CH2
νas 2940
νsym 2870
a)
b)
c)
0.0
0.5
1.0
1.5
3800
3600
3400
3200
3000
2800
2600

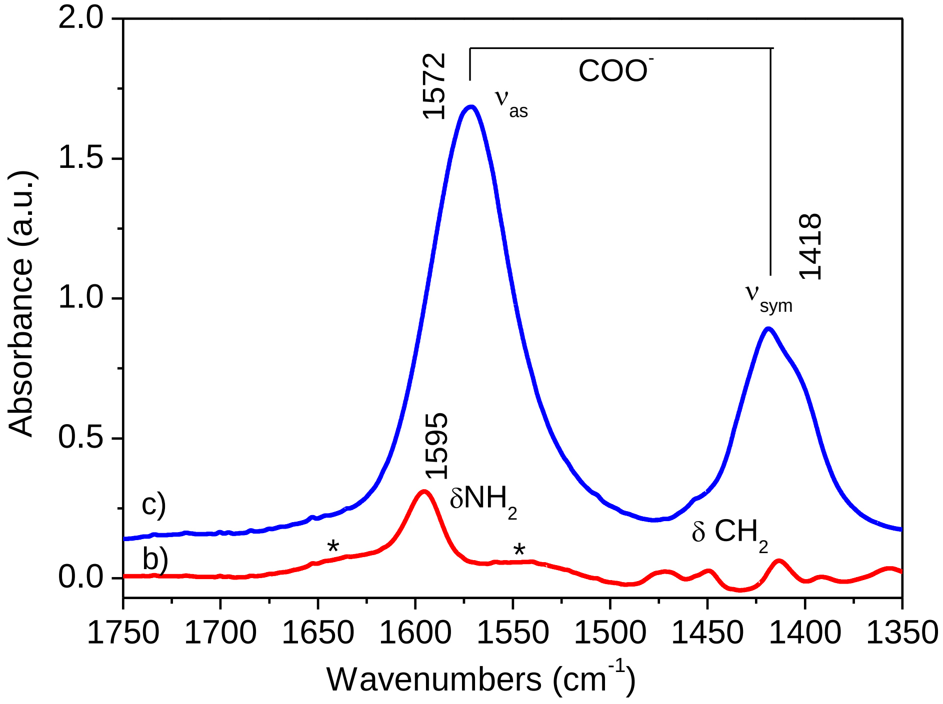
Absorbance (a.u.)
Wavenumbers (cm-1)
1572 νas
COO-
1418 νsym
1595
δNH2
δ CH2
c)
b)
*
*
0.0
0.5
1.0
1.5
2.0
1750
1700
1650
1600
1550
1500
1450
1400
1350

Figure 4

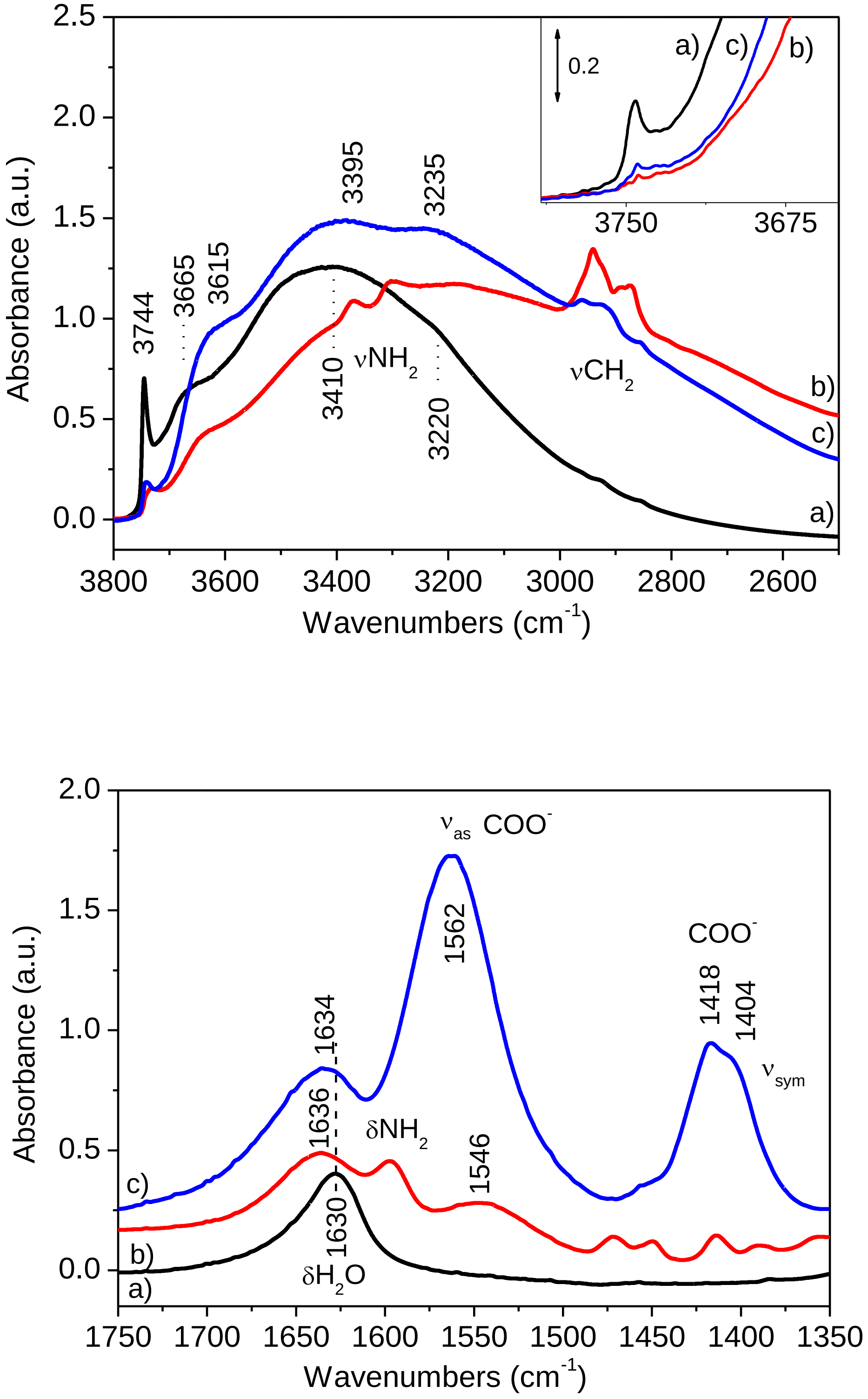
Absorbance (a.u.)
2.5
2.0
1.5
1.0
0.5
0.0
3744
3665
3615
3395
3235
3410
3220
νNH$_2$
νCH$_2$
a)
b)
c)
0.2
3750
3675
3800
3600
3400
3200
3000
2800
2600
Wavenumbers (cm^{-1})
Absorbance (a.u.)
2.0
1.5
1.0
0.5
0.0
ν$_{as}$ COO$^-$
1562
COO$^-$
1418
1404
ν$_{sym}$
1634
1636
δNH$_2$
1546
1630
δH$_2$O
1750
1700
1650
1600
1550
1500
1450
1400
1350
Wavenumbers (cm^{-1})

Figure 5

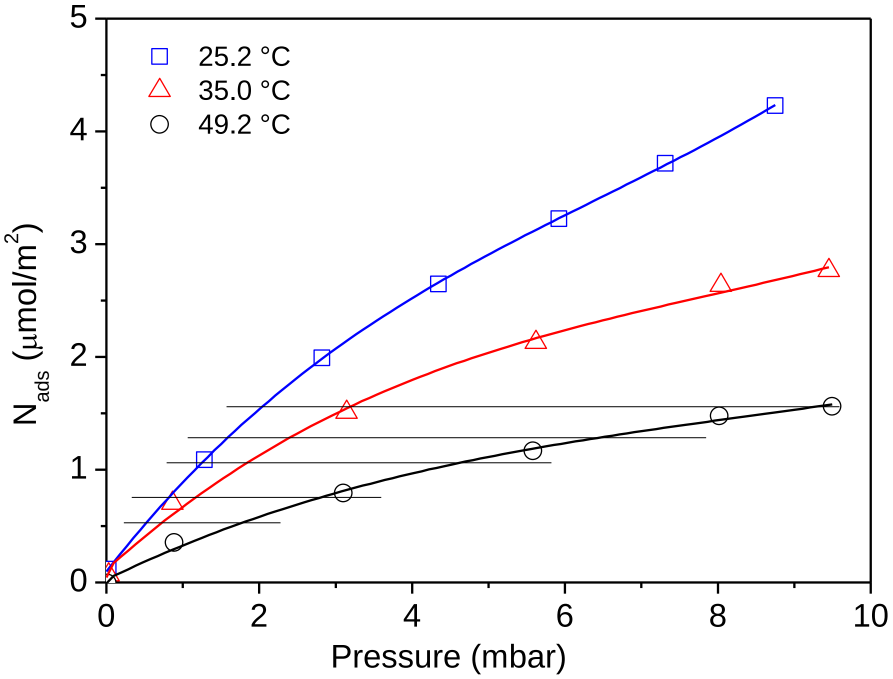

Figure 6

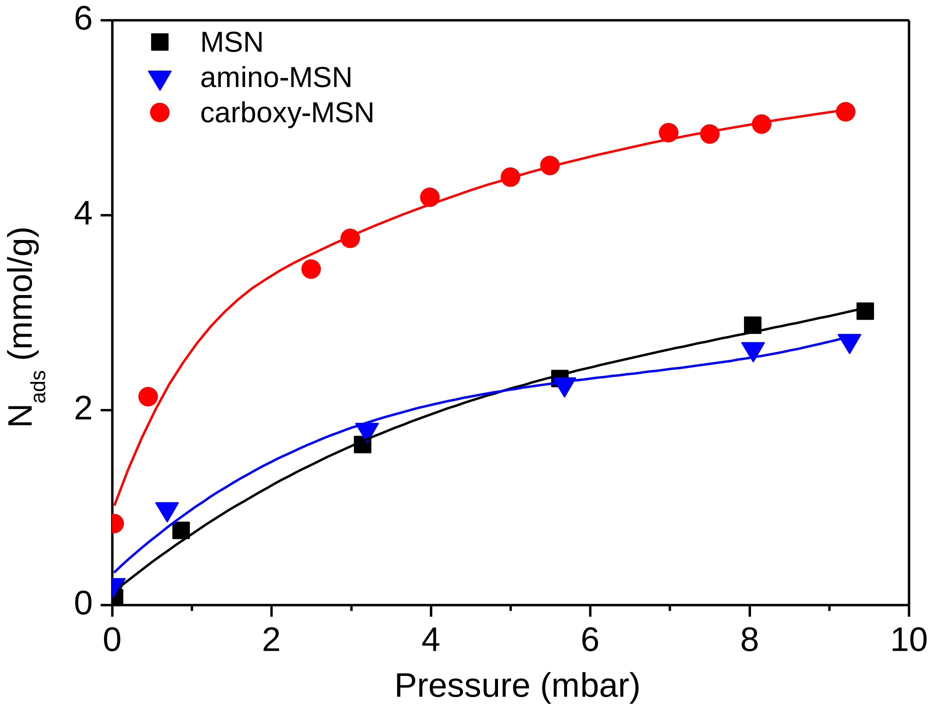
MSN
amino-MSN
carboxy-MSN
N_{ads} (mmol/g)
Pressure (mbar)
0
2
4
6
0
2
4
6
8
10

Figure 7

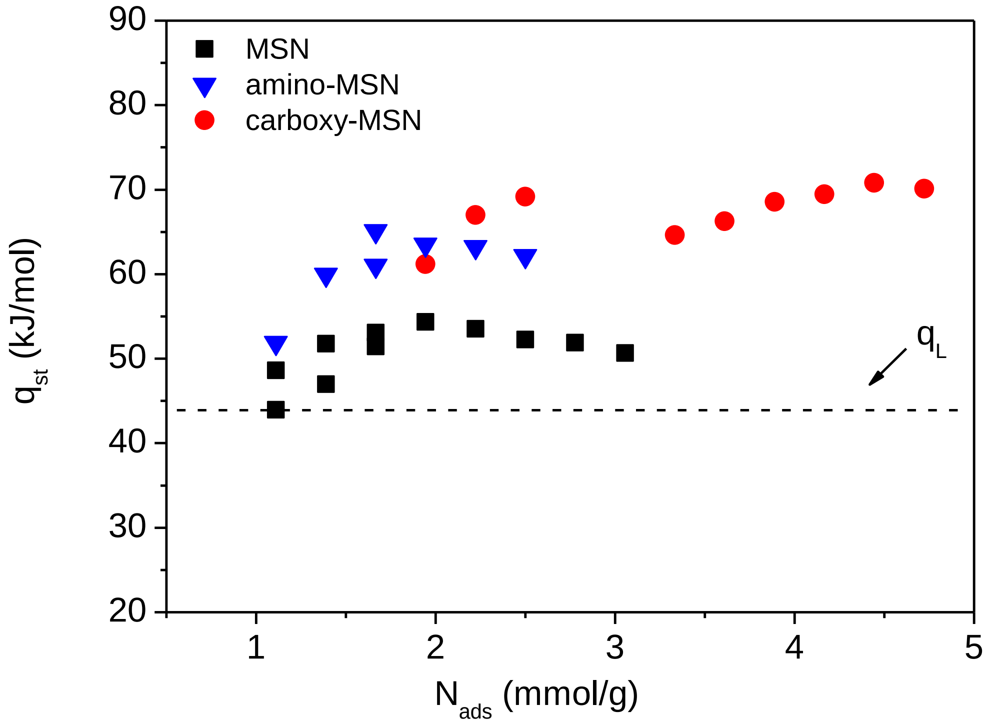
90
80
70
60
50
40
30
20
1
2
3
4
5
■ MSN
▼ amino-MSN
● carboxy-MSN
q_L
q_{st} (kJ/mol)
N_{ads} (mmol/g)

Figure 8

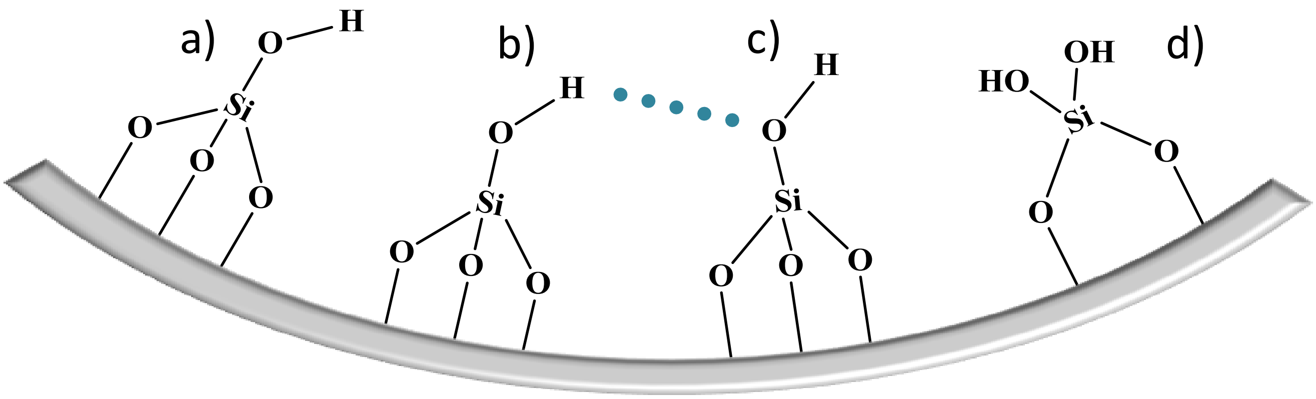

Scheme 1 Schematic view of possible silanol groups on the inner surface of MSN: a) isolated, b) and c) H- bonding interacting (donor and acceptor, respectively), d) geminal.

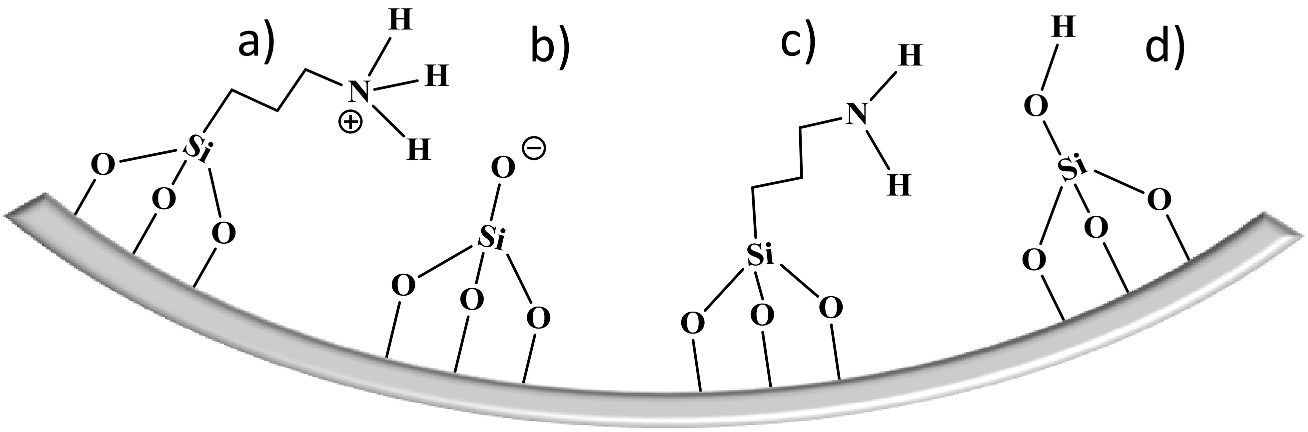

Scheme 2 Schematic view of possible groups present on the surface of amino-MSN pore walls: a) and b) ammoniumpropyl/silanolate,[69] c) aminopropyl and d) silanol. For simplicity anchoring groups are represented as tri-legged siloxanes, even if the presence of mono- (-Si(OH)$_2$R) and bi-legged (=Si(OH)R) species cannot be excluded.[64-66]

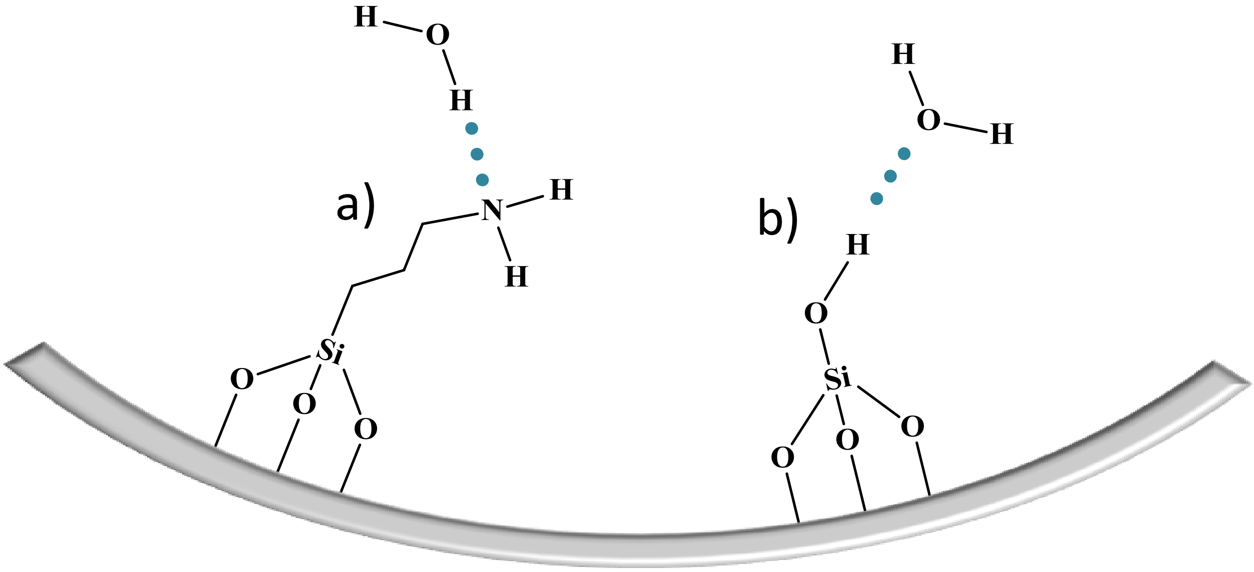

Scheme 3 Schematic view of possible H-bonding interactions of single water molecules with a) aminopropyl and b) silanol groups on the pore surface of amino-MSN.

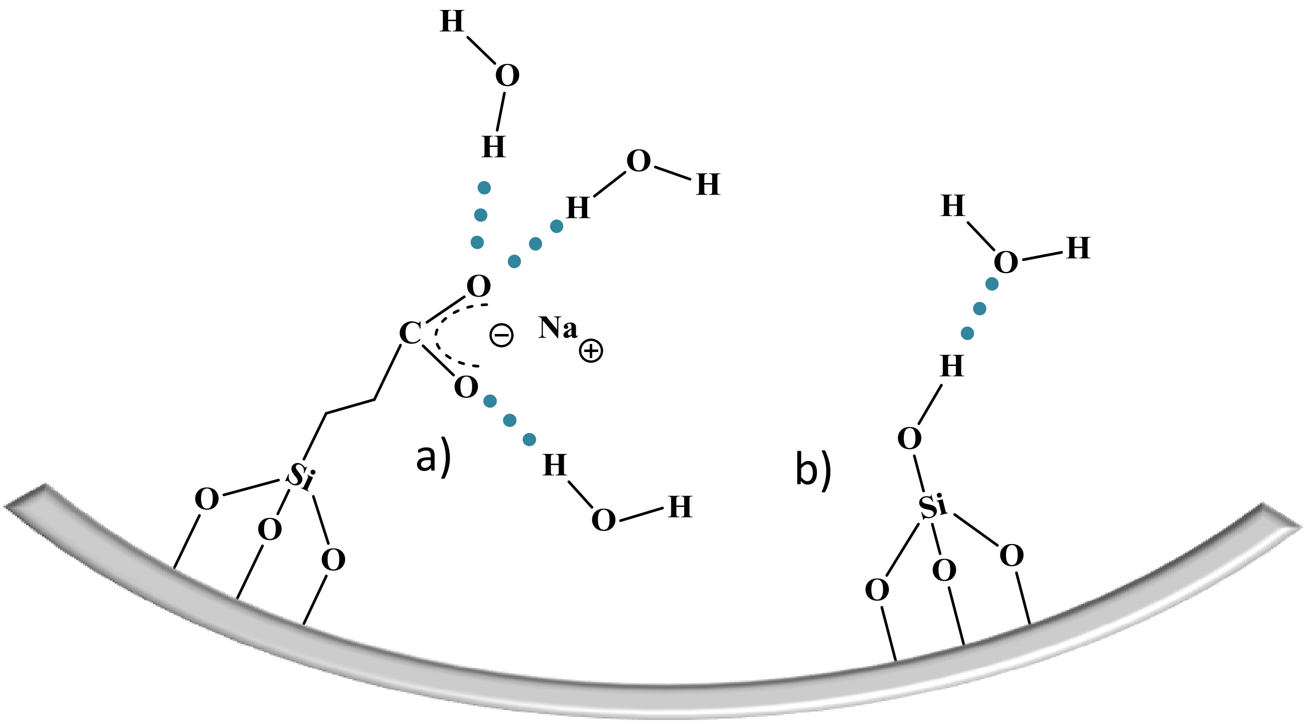

Scheme 4 Schematic view of possible H-bonding interactions of water molecules with a) sodium ethylcarboxylate and b) silanols groups on the pore surface of carboxy-MSN. In case a) three water molecules were depicted to suggest the possibility of multiple H-bonding interactions (see text and Ref. 76).